

# Application of Compact-Reconstruction Weighted Essentially Nonoscillatory Schemes to Compressible Aerodynamic Flows

Debojyoti Ghosh,\* Shivaji Medida,† and James D. Baeder‡  
*University of Maryland, College Park, Maryland 20742*

DOI: 10.2514/1.J052654

Compact-reconstruction weighted essentially nonoscillatory schemes have lower dissipation and dispersion errors as well as higher spectral resolution than weighted essentially nonoscillatory schemes of the same order of convergence. Numerical experiments on benchmark inviscid flow problems have demonstrated improvements in the resolution and preservation of flow features such as vortices, discontinuities, and small-length-scale waves. This paper describes the integration of these schemes with a compressible, unsteady, Reynolds-averaged Navier-Stokes solver and demonstrates their performance for two- and three-dimensional flow problems. The schemes are validated and verified for domains discretized by curvilinear and overset grids. Several flow examples demonstrate improvements in the resolution of boundary-layer and wake-flow features for solutions obtained by the compact-reconstruction weighted essentially nonoscillatory schemes. The results presented indicate that these schemes are well suited to aerodynamic problems where high-resolution numerical solutions of the near-body and wake flowfields are desired.

## Nomenclature

$A$	= flux Jacobian
$c$	= optimal weights or airfoil chord
$e$	= internal energy
$F$	= convective flux tensor
$F^v$	= viscous flux tensor
$f, g, h$	= convective flux vector along $x, y, z$ , axis
$f^v, g^v, h^v$	= viscous flux vector along $x, y, z$ axis
$i, j, k$	= grid indices or dimension indices
$\hat{i}, \hat{j}, \hat{k}$	= unit vectors along Cartesian directions
$M$	= Mach number
$Pr$	= Prandtl number
$p$	= pressure
$q$	= thermal conduction
$Re$	= Reynolds number
$S$	= source term
$t$	= time
$u$	= conserved variable vector
$u, v, w$	= velocity along $x, y, z$ axis
$X$	= matrix of eigenvectors
$x, y, z$	= Cartesian coordinates
$\beta$	= smoothness indicators
$\delta$	= Kronecker delta function
$\Lambda$	= matrix of eigenvalues
$\mu$	= coefficient of viscosity
$\rho$	= density
$\tau$	= viscous stress
$\omega$	= weighted essentially nonoscillatory weights

## I. Introduction

THE Navier-Stokes equations govern the dynamics of viscous, compressible flows [1] and constitute a system of nonlinear hyperbolic-parabolic conservation laws. Solutions to these equations are composed of waves traveling at their characteristic speeds. The nonlinearity of the convective terms implies that solutions may admit discontinuities and steep gradients such as shock waves and shear layers. Numerical schemes for the Navier-Stokes equations need to respect the wave nature of the solution as well as ensure nonoscillatory behavior across discontinuities. Several such methods have been proposed in the literature [1,2] and applied to aerodynamic flows. The focus of this paper is the high-resolution numerical solution to aerodynamic flows characterized by a large range of length scales, where, in addition to the accurate prediction of integrated forces, a well-resolved solution to the flowfield is desired as well.

The essentially nonoscillatory (ENO) schemes [3] use adaptive stenciling to avoid oscillations across discontinuities by choosing the smoothest interpolation stencil amongst the candidates. The implementation of the ENO schemes was improved and extended [4,5] and applied to several benchmark flow problems. The weighted essentially nonoscillatory (WENO) schemes [6] replaced the selection procedure of the ENO schemes with a weighted combination of the candidate interpolation schemes and achieved a higher order of accuracy for the same computational expense. The WENO schemes were improved [7] such that they achieved  $(2r - 1)$ -th-order accuracy corresponding to the  $r$ th-order ENO scheme. WENO schemes of very high orders of accuracy have been constructed and applied to benchmark flow problems [8]. Improvements to the nonlinear weights [9–11] addressed several drawbacks, such as suboptimal convergence for a class of smooth solutions as well as excessive dissipation across discontinuities. The WENO schemes have been applied to a large range of flow problems and other physical systems governed by hyperbolic conservation laws [12].

One of the primary drawbacks of high-order WENO schemes (and other noncompact schemes) is the low spectral resolution, and this is a severe limitation for flows with a large range of length scales. Compact finite-difference schemes [13] have significantly higher spectral resolution and lower dissipation and dispersion errors, compared to noncompact schemes, as well as smaller interpolation stencils. These schemes have been applied to several incompressible [14,15] and compressible [16,17] flow problems. Linear compact schemes result in spurious oscillations across discontinuities, and a shock-capturing compact scheme with a total variation bounded limiter was introduced [18] and further improved [19].

Presented as Paper 2012-2832 at the 42nd AIAA Fluid Dynamics Conference and Exhibit, New Orleans, LA, 25–28 June 2012; received 2 March 2013; revision received 31 March 2014; accepted for publication 28 April 2014; published online 21 July 2014. Copyright © 2014 by the American Institute of Aeronautics and Astronautics, Inc. All rights reserved. Copies of this paper may be made for personal or internal use, on condition that the copier pay the \$10.00 per-copy fee to the Copyright Clearance Center, Inc., 222 Rosewood Drive, Danvers, MA 01923; include the code 1533-385X/14 and \$10.00 in correspondence with the CCC.

\*Graduate Research Assistant, Applied Mathematics & Statistics, and Scientific Computation.

†Graduate Research Assistant, Aerospace Engineering.

‡Associate Professor, Aerospace Engineering. Associate Fellow AIAA.

There have been several efforts in the literature that attempt to construct a nonoscillatory scheme with high spectral resolution by combining the ENO or WENO schemes and the compact schemes. The hybrid schemes [20–22] are one such family of schemes, where the local smoothness of the solution is used to select the ENO or WENO scheme and a compact scheme. A parameter-free compact-WENO scheme was proposed [23] where the WENO scheme at discontinuities acts as internal boundaries to the compact scheme. One drawback of these approaches is that the schemes revert to a noncompact scheme (with poor spectral resolution) around discontinuities, resulting in a loss of accuracy and resolution. This is exacerbated for flows with a large number of discontinuities (e.g., shocklets) because the hybrid algorithm would select the noncompact ENO or WENO scheme in the majority of the domain. Another class of schemes [24,25] involves two stages on a staggered grid. The first stage interpolates the flux at the interfaces with the WENO scheme, and the second stage computes higher-order approximations to the first derivative from the interface values with central compact schemes. A similar ENO-Padé scheme [26] achieved higher orders of accuracy at both stages of the reconstruction step. The spectral resolution of these schemes is only marginally higher than the WENO schemes because they use a noncompact scheme to compute the interface fluxes. A weighted compact scheme was constructed [27] that uses a weighted combination of candidate compact schemes to construct a high-order accurate, nonoscillatory scheme. The candidate schemes are chosen as third- and fourth-order compact schemes, and the optimal scheme is a sixth-order central scheme that is inherently unstable for hyperbolic problems. The overall scheme was not robust, and further treatments like an additional filter [28] or hybridization with a noncompact scheme [29] were necessary to obtain nonoscillatory solutions.

A class of robust, weighted, nonlinear compact schemes have been introduced [30] that have a high spectral resolution and yield nonoscillatory solutions across discontinuities. The compact-reconstruction weighted essentially nonoscillatory (CRWENO) schemes are constructed by identifying lower-order compact interpolation schemes at each grid interface as well as corresponding optimal weights such that the weighted sum is a higher-order accurate upwind compact scheme. These optimal weights are replaced by the smoothness-dependent WENO weights [7] such that they approach their optimal values for smooth solutions and vanish near discontinuities. The resulting CRWENO scheme is high-order accurate for smooth flows and nonoscillatory across discontinuities and steep gradients without additional numerical treatments. Fifth-order CRWENO schemes were constructed [30] and their numerical properties demonstrated on scalar conservation laws and the inviscid Euler equations.

The fifth-order CRWENO schemes have several advantages over the fifth-order WENO scheme. The CRWENO schemes yield solutions with significantly lower dissipation and dispersion errors; thus, significant improvements were observed in their ability to preserve flow features as they convect over large distances. The higher spectral resolution of the CRWENO schemes substantially improved the resolution of small-length-scale flow features as well as extrema and discontinuities. The CRWENO schemes were demonstrated to be computationally more efficient for scalar conservation laws and the Euler equations with componentwise reconstruction of the vector quantities. These improvements in the numerical properties were demonstrated [30] on the linear advection equations as well as benchmark one- and two-dimensional inviscid flow problems on equispaced Cartesian grids. The CRWENO schemes were applied to the direct numerical simulation of compressible turbulent flows [31] and yielded solutions with improved resolution of small and moderate length scales. These results indicate that the CRWENO schemes are expected to show improvements over the WENO scheme for flow problems characterized by a large range of length scales and long-term convection of flow features. This paper describes the incorporation of the fifth-order CRWENO scheme into an unsteady, compressible Reynolds-averaged Navier–Stokes solver for curvilinear and overset grids and its application to several two- and three-dimensional aerodynamic problems.

The outline of this paper is as follows. Section II describe the three-dimensional, compressible Navier–Stokes equations in their nondimensionalized form. The numerical method and the fifth-order CRWENO scheme are described in Sec. III. Several flow problems are presented in Sec. IV. The CRWENO scheme is validated for steady and unsteady flows around two-dimensional airfoils and a three-dimensional wing and a rotor. The examples presented in this paper have a large range of length scales, from airfoil chord length or blade span to boundary-layer thickness or the diameter of shed vortices. A lower-order numerical scheme is sufficient for the prediction of integrated forces, but a high-order accurate scheme is required to obtain a well-resolved solution to the flowfield. The performance of the CRWENO scheme is assessed and compared with that of the WENO scheme, with the primary focus on the ability to resolve and preserve small-length-scale flow features such as shed vortices. Conclusions are drawn in Sec. V.

## II. Governing Equations

The three-dimensional, compressible Navier–Stokes equations [1] are expressed in their nondimensional form as

$$\frac{\partial \mathbf{u}}{\partial t} + \frac{\partial \mathbf{f}}{\partial x} + \frac{\partial \mathbf{g}}{\partial y} + \frac{\partial \mathbf{h}}{\partial z} = \frac{\partial \mathbf{f}^v}{\partial x} + \frac{\partial \mathbf{g}^v}{\partial y} + \frac{\partial \mathbf{h}^v}{\partial z} + S \quad (1)$$

where  $\mathbf{u}$  is the vector of conserved variables;  $\mathbf{f}$ ,  $\mathbf{g}$ , and  $\mathbf{h}$  are the convective flux vectors;  $\mathbf{f}^v$ ,  $\mathbf{g}^v$ , and  $\mathbf{h}^v$  are the viscous flux vectors; and  $S$  is a source term representing body forces. In this paper, the pseudoforces resulting from formulating the equations in a noninertial frame are included in the source term. The conserved variables and the convective flux vectors are

$$\begin{aligned} \mathbf{u} &= \begin{bmatrix} \rho \\ \rho u \\ \rho v \\ \rho w \\ e \end{bmatrix}, \quad \mathbf{f} = \begin{bmatrix} \rho u \\ \rho u^2 + p \\ \rho uv \\ \rho uw \\ (e + p)u \end{bmatrix}, \quad \mathbf{g} = \begin{bmatrix} \rho v \\ \rho uv \\ \rho v^2 + p \\ \rho vw \\ (e + p)v \end{bmatrix}, \\ \mathbf{h} &= \begin{bmatrix} \rho w \\ \rho uw \\ \rho vw \\ \rho w^2 + p \\ (e + p)w \end{bmatrix} \end{aligned} \quad (2)$$

and the viscous fluxes are

$$\begin{aligned} \mathbf{f}^v &= \begin{bmatrix} 0 \\ \tau_{xx} \\ \tau_{yx} \\ \tau_{zx} \\ u\tau_{xx} + v\tau_{yx} + w\tau_{zx} - q_x \end{bmatrix}, \\ \mathbf{g}^v &= \begin{bmatrix} 0 \\ \tau_{xy} \\ \tau_{yy} \\ \tau_{zy} \\ u\tau_{xy} + v\tau_{yy} + w\tau_{zy} - q_y \end{bmatrix}, \\ \mathbf{h}^v &= \begin{bmatrix} 0 \\ \tau_{xz} \\ \tau_{yz} \\ \tau_{zz} \\ u\tau_{xz} + v\tau_{yz} + w\tau_{zz} - q_z \end{bmatrix} \end{aligned} \quad (3)$$

The equation of state is given by

$$e = \frac{p}{\gamma - 1} + \frac{1}{2}\rho(u^2 + v^2 + w^2) \quad (4)$$

The mean viscous stresses are

$$\tau_{ij} = \frac{\mu M_\infty}{Re_\infty} \left[ \left( \frac{\partial u_i}{\partial x_j} + \frac{\partial u_j}{\partial x_i} \right) - \frac{2}{3} \frac{\partial u_k}{\partial x_k} \delta_{ij} \right] \quad (5)$$

where  $Re_\infty$  and  $M_\infty$  are the freestream Reynolds number and Mach number, and  $\mu$  is the nondimensionalized coefficient of laminar viscosity. The thermal conduction terms are

$$q_i = -\frac{\mu M_\infty}{Re_\infty Pr(\gamma - 1)} \frac{\partial T}{\partial x_i} \quad (6)$$

where  $Pr$  is the Prandtl number, which is assumed as 0.72 (constant) for all flow problems in this paper.

Turbulent flows are modeled using the Reynolds-averaged Navier–Stokes (RANS) formulation [1], and additional terms for the Reynolds stress tensor are included in the momentum and energy equations to account for the momentum and energy exchange due to turbulent fluctuations. In this paper, the one-equation Spalart–Allmaras turbulence model [32] with the rotational correction [33] is used to close the system of equations.

### III. Numerical Methodology

The unsteady, compressible RANS equations form a hyperbolic–parabolic system of partial differential equations where the equations are hyperbolic without the viscous terms and parabolic without the convective terms. Equation (1) is transformed to its integral form by integrating over a control volume and applying the Stokes theorem. The finite-volume formulation [34] is used to discretize it in space, resulting in an ordinary differential equation in time:

$$\frac{d\bar{\mathbf{u}}}{dt} + \frac{1}{V} \sum_{l=0}^{N_{\text{faces}}} \mathbf{F}_l \cdot \mathbf{n}_l dS_l = \frac{1}{V} \sum_{l=0}^{N_{\text{faces}}} F_l^v \cdot \hat{\mathbf{n}}_l dS_l + \bar{S} \quad (7)$$

where  $\bar{\mathbf{u}}$  and  $\bar{S}$  are the volume-averaged conserved variables and source term in a grid cell (control volume),  $V$  is the volume of the grid cell,  $N_{\text{faces}}$  is the number of discrete interfaces of the grid cell,  $\hat{\mathbf{n}}$  is the unit normal vector for a given interface, and  $dS$  is the interface area. The convective and viscous flux tensors are given by

$$\mathbf{F} = f\hat{\mathbf{i}} + g\hat{\mathbf{j}} + h\hat{\mathbf{k}} \quad \mathbf{F}^v = f^v\hat{\mathbf{i}} + g^v\hat{\mathbf{j}} + h^v\hat{\mathbf{k}} \quad (8)$$

where  $\hat{\mathbf{i}}, \hat{\mathbf{j}}, \hat{\mathbf{k}}$  are the Cartesian unit vectors. Thus, the finite-volume discretization requires the reconstruction of the convective and viscous flux vectors at the interfaces from the cell-averaged values. This is described in more details in the following subsection for the convective flux vector. The viscous terms are approximated using second-order central finite-difference approximations. Viscous flow problems need very fine mesh spacing to resolve the boundary layers, and this results in restrictive stability limits for explicit time-marching schemes. In this study, Eq. (7) is evolved in time using the implicit, second-order accurate backward-differencing scheme. The resulting system of equations is solved using the diagonalized alternate direction implicit [35,36] or the lower-upper Symmetric Gauss–Seidel [37,38] schemes. Dual time stepping [39] is used for time-accurate solutions to unsteady problems.

#### A. Reconstruction

The three-dimensional domain is discretized with a structured grid, and thus, to solve Eq. (7), the reconstruction step computes the convective flux at  $(i \pm 1/2, j, k)$ ,  $(i, j \pm 1/2, k)$ , and  $(i, j, k \pm 1/2)$  (cell interfaces) for the  $(i, j, k)$ th grid cell (where  $i, j, k$  are the grid indices). The reconstruction of this flux vector at the  $(i + 1/2, j, k)$ th

interface is described in this section and the flux vectors at the other interfaces are similarly computed. At the interface, a one-dimensional reconstruction is carried out along the grid coordinate normal to the interface, independent of the other grid coordinates. In the following description, the corresponding grid index  $i$  is retained, and the other two indices  $j, k$  are dropped. The wave nature of the hyperbolic convective flux terms is modeled through the process of upwinding, and the Roe scheme [40] with the Harten entropy fix [3] is used in this study. The interface flux is expressed as

$$\hat{\mathbf{F}}_{n,i+1/2} = \frac{1}{2} (\hat{\mathbf{F}}_{n,i+1/2}^L + \hat{\mathbf{F}}_{n,i+1/2}^R) - \frac{1}{2} |A(\hat{\mathbf{u}}_{i+1/2}^L, \hat{\mathbf{u}}_{i+1/2}^R)| (\hat{\mathbf{u}}_{i+1/2}^L + \hat{\mathbf{u}}_{i+1/2}^R) \quad (9)$$

where  $\mathbf{F}_n = \mathbf{F} \cdot \mathbf{n}$  is the flux vector normal to the interface, the hat denotes the numerical (interpolated) approximation of the corresponding quantities, and

$$|A(\hat{\mathbf{u}}_{i+1/2}^L, \hat{\mathbf{u}}_{i+1/2}^R)| = X_{i+1/2} |\Lambda_{i+1/2}| X_{i+1/2}^{-1} \quad (10)$$

The eigenvalues  $\Lambda$  and eigenvectors  $X, X^{-1}$  are evaluated normal to the interface [41] from the Roe-averaged flow quantities at the interface. The superscripts  $L$  and  $R$  denote left- and right-biased interpolated values, respectively, and Eq. (9) requires these interpolated values of the flux  $\hat{\mathbf{F}}$  and conserved variable  $\hat{\mathbf{u}}$  vectors at the interface ( $i + 1/2$ ). In this study, the fifth-order CRWENO scheme [30] (CRWENO5) is used to interpolate the flux and conserved variable vectors at the interfaces. The formulation of this compact scheme is briefly described for a scalar quantity in the following subsection, and its application to the vector quantities in Eq. (9) is then discussed. The numerical properties of the CRWENO5 scheme are compared with those of two noncompact schemes: the third-order MUSCL scheme [42] with Koren’s limiter [43] (MUSCL3), and the fifth-order WENO scheme [7] (WENO5).

#### B. Fifth-Order Compact-Reconstruction Weighted Essentially Nonoscillatory Scheme

The one-dimensional, left-biased interpolation of a scalar function  $f(x)$  using the CRWENO5 scheme is briefly described next and the corresponding right-biased interpolation scheme can be easily derived. The extensions to the Navier–Stokes system of equations are discussed subsequently. The fifth-order CRWENO scheme is constructed by identifying three third-order compact interpolation schemes at a given interface:

$$\frac{2}{3} \hat{f}_{i-1/2} + \frac{1}{3} \hat{f}_{i+1/2} = \frac{1}{6} (f_{i-1} + 5f_i); \quad c_1 = \frac{2}{10} \quad (11)$$

$$\frac{1}{3} \hat{f}_{i-1/2} + \frac{2}{3} \hat{f}_{i+1/2} = \frac{1}{6} (5f_i + f_{i+1}); \quad c_2 = \frac{5}{10} \quad (12)$$

$$\frac{2}{3} \hat{f}_{i+1/2} + \frac{1}{3} \hat{f}_{i+3/2} = \frac{1}{6} (f_i + 5f_{i+1}); \quad c_3 = \frac{3}{10} \quad (13)$$

The optimal weights  $c_k; k = 1, \dots, 3$  are such that the weighted sum of these interpolation schemes results in a fifth-order accurate compact interpolation scheme:

$$\frac{3}{10} \hat{f}_{i-1/2} + \frac{6}{10} \hat{f}_{i+1/2} + \frac{1}{10} \hat{f}_{i+3/2} = \frac{1}{30} f_{i-1} + \frac{19}{30} f_i + \frac{1}{3} f_{i+1} \quad (14)$$

The CRWENO5 scheme is obtained by replacing the optimal weights  $c_k$  with nonlinear WENO weights  $\omega_k$  and is thus expressed as

$$\begin{aligned} & \left( \frac{2}{3}\omega_1 + \frac{1}{3}\omega_2 \right) \hat{f}_{i-1/2} + \left[ \frac{1}{3}\omega_1 + \frac{2}{3}(\omega_2 + \omega_3) \right] \hat{f}_{i+1/2} + \frac{1}{3}\omega_3 \hat{f}_{i+3/2} \\ & = \frac{\omega_1}{6} f_{i-1} + \frac{5(\omega_1 + \omega_2) + \omega_3}{6} f_i + \frac{\omega_2 + 5\omega_3}{6} f_{i+1} \end{aligned} \quad (15)$$

This results in a tridiagonal system of equations. In the current implementation, the definition of the nonlinear weights is identical to that for the WENO schemes [7]. The weights are defined as

$$\omega_k = \frac{\alpha_k}{\sum_k \alpha_k}; \quad \alpha_k = \frac{c_k}{(\epsilon + \beta_k)^p}; \quad i = 1, \dots, 3 \quad (16)$$

where  $\epsilon = 10^{-6}$  is a small number to prevent division by zero, the optimal weights  $c_k$  are defined in Eqs. (11–13), and  $\beta_k$  are smoothness indicators defined as follows:

$$\beta_1 = \frac{13}{12} (f_{i-2} - 2f_{i-1} + f_i)^2 + \frac{1}{4} (f_{i-2} - 4f_{i-1} + 3f_i)^2 \quad (17)$$

$$\beta_2 = \frac{13}{12} (f_{i-1} - 2f_i + f_{i+1})^2 + \frac{1}{4} (f_{i-1} - f_{i+1})^2 \quad (18)$$

$$\beta_3 = \frac{13}{12} (f_i - 2f_{i+1} + f_{i+2})^2 + \frac{1}{4} (3f_i - 4f_{i+1} + f_{i+2})^2 \quad (19)$$

Although the stencils for the WENO smoothness indicators differ from those of the CRWENO5 scheme, numerical results presented in [30] as well as this paper indicate that the resulting scheme is high-order accurate and nonoscillatory.

Boundary closure for the CRWENO5 scheme is implemented by extending the domain with ghost cells and applying the WENO5 scheme [7] at the first and last interfaces. Assuming the optimal values for the weights, this is expressed as

$$i = 0: \hat{f}_{1/2} = \frac{1}{30} f_{-2}^G - \frac{13}{60} f_{-1}^G + \frac{47}{60} f_0^G + \frac{27}{60} f_1 - \frac{1}{20} f_2 \quad (20)$$

$$\begin{aligned} i = 1, \dots, N-1: & \frac{3}{10} \hat{f}_{i-1/2} + \frac{6}{10} \hat{f}_{i+1/2} + \frac{1}{10} \hat{f}_{i+3/2} \\ & = \frac{1}{30} f_{i-1} + \frac{19}{30} f_i + \frac{1}{3} f_{i+1} \end{aligned} \quad (21)$$

$$i = N: \hat{f}_{N+1/2} = \frac{1}{30} f_{N-2} - \frac{13}{60} f_{N-1} + \frac{47}{60} f_N + \frac{27}{60} f_{N+1}^G - \frac{1}{20} f_{N+2} \quad (22)$$

where the superscript  $G$  denotes ghost points, and  $N$  is the number of grid points inside the domain. The conserved variables in the ghost points are specified in a manner consistent with the physical boundary conditions, and the corresponding fluxes are known.

### C. Discussion

The numerical properties of the fifth-order CRWENO scheme was studied [30,44] for scalar conservation laws as well as the Euler equations. The compact scheme has several advantages over the non-compact WENO scheme of the same order of convergence. Taylor series analysis indicate that dissipation and dispersion errors for the CRWENO5 scheme are 1/10 and 1/15 those of the WENO5 scheme for smooth solutions. Numerical experiments on the linear advection equation and the inviscid Euler equations demonstrated that the CRWENO5 scheme yields solutions with significantly lower errors than the WENO5 scheme for both smooth problems as well as problems with discontinuities. The higher spectral resolution of the compact scheme results in lower dissipation and phase errors over a larger range of length scales. The numerical cost of the CRWENO5 scheme was also analyzed, and though this scheme is more expensive than the WENO5 scheme for the same grid size, the lower errors

allow solutions of similar accuracy to be obtained on considerably coarser grids. In general, the fifth-order CRWENO scheme yields solutions that are comparable to solutions obtained by the fifth-order WENO scheme on a grid that is 1.5 times as fine. Thus, the CRWENO5 scheme was demonstrated to be more efficient through specific examples [30,44]. Based on these results, the scheme is applied to practical aerodynamic flow problems in this paper where the superior numerical properties are expected to yield well-resolved flowfield solutions.

The scalar interpolation schemes described in the preceding section can be extended to the vector quantities in Eq. (9) in two possible ways: componentwise reconstruction and characteristic-based reconstruction. A characteristic-based reconstruction results in a more robust numerical scheme and is necessary to yield nonoscillatory solutions to inviscid flows with strong discontinuities [7]. However, a study of the numerical cost of the CRWENO5 scheme for the inviscid Euler equations [30,44] showed that, although this scheme is computationally more efficient than the WENO5 scheme for a componentwise reconstruction, it is not so for a characteristic-based reconstruction. This is due to the requirement of solving a block tridiagonal system at each iteration, when the scheme is applied along the characteristics. However, it was also observed in the case of the advection of an entropy wave and the convection of an isentropic vortex that the componentwise reconstruction yielded solutions identical to the characteristic-based reconstruction. It is shown through a number of examples in this paper that the componentwise reconstruction yields accurate solutions in the presence of physical viscosity and/or in the absence of strong discontinuities, and thus the CRWENO5 scheme is applicable to such problems. Numerical results presented in this paper are all obtained by applying the CRWENO5, WENO5, and MUSCL3 schemes through a componentwise reconstruction.

### D. Application to Overset Grids

Flow problems in complicated domains are often solved on overset grids that may have relative motion specified. Numerical algorithms for such domains need to identify regions for each mesh that contain field points or are blanked out or marked as an overlap region. The governing equations are solved on the field points, whereas in the overlap region, the solution is transferred from a different grid; the overlap region thus serves as an internal “boundary”. The blanked-out region (“hole”) is ignored by the solution algorithm and thus contains nonphysical flow values. This involves a three-step process: hole-cutting, identification of the blanked-out and overlap points, and finding donor cells and interpolation coefficients for the transfer of solution between the grids. In this work, the implicit hole-cutting algorithm [45] is used to identify the blanked-out and overlap regions and find donor cells for the receiver cells in the overlap region of each grid. A bi- or trilinear interpolation is used to compute the flow values in the overlap region from the solution at the donor cells. Higher-order interpolation based on Langrangian polynomials and B-splines has been applied [46] because the second-order interpolation compromises the accuracy of the global solution. Thus, one future direction of work is the implementation of these higher-order interpolation schemes in the current algorithm.

The implementation of noncompact spatial reconstruction schemes to overset grids is relatively straightforward. The numerical algorithm does not solve the governing equations on the blanked-out points, and the flow values at these points are nonphysical. However, field points are insulated from these blanked-out points through the overlap region, whose thickness corresponds to the stencil width of the spatial reconstruction scheme. Thus, the nonphysical flow values in the blanked-out region do not contaminate the reconstruction step at the field points. However, the implementation of a compact scheme is not straightforward. A compact scheme results in a coupled formulation for the unknown interface fluxes; for example, Eq. (14) or Eq. (15) represents tridiagonal systems of equations. As a result, the unknown fluxes at the interfaces inside the blanked-out region are coupled to those in the field region. Thus, the application of compact schemes to overset grids requires some special treatment to effectively decouple

the system of equations from the variables inside the blanked-out region. One approach to this is the application of biased compact interpolation schemes at points near the hole boundaries [46], thereby decoupling the global system of equations from the grid points in the holes.

The CRWENO5 scheme achieves this decoupling through the same solution-dependent stencil-selection mechanism that avoids discontinuities. Examination of Eq. (15) shows that, when the weight corresponding to the constituent third-order scheme with a discontinuity in its stencil goes to zero, the scheme reduces to a bidiagonal equation for that interface, biased away from the discontinuity. This results in a decoupling of the system of equations across each discontinuity [44], thus avoiding oscillations. It is expected that the nonphysical values inside the blanked-out region will cause the CRWENO5 scheme to see its boundary as a discontinuity. Therefore, the weights corresponding to the third-order schemes with stencils crossing into the hole region will go to zero, resulting in a bidiagonal scheme biased away from the blanked-out points. This will effectively decouple the reconstruction at the field points from the hole region, thus preventing contamination. Thus, the CRWENO5 scheme is expected to be applicable to overset grids without additional modifications. This is verified for both two- and three-dimensional flows in Secs. IV.B, IV.E.

#### E. Parallelization

Section IV.E considers a three-dimensional domain with  $\sim 3$  million points, and the solutions are obtained on multiple processors. The implementation in this paper uses a splitting approach [47] where the global system of equations (resulting from the compact scheme) is replaced by independent systems in each local subdomain. This is possible by applying the noncompact WENO scheme (of the same order of accuracy) at the parallel-partitioning boundaries. One major drawback of this approach is that the numerical properties of the overall algorithm is a function of the number of processors. This is evaluated and described in details for the parallel hybrid compact-WENO scheme [47]. The simulations in this paper are carried on very few number of processors with large local subdomains, and thus parallelization-induced errors are negligible. Recent work [48] describe an efficient and scalable parallel implementation of the CRWENO scheme for massively parallel computations with very small local subdomain sizes.

### IV. Numerical Results

This section presents several flow problems that validate the CRWENO5 scheme for curvilinear and overset grids as well as demonstrate its numerical properties. The steady flow around the RAE2822 airfoil is considered to validate the scheme for a curvilinear grid. The unsteady flow around a pitching SC1095 airfoil in a wind tunnel is solved to validate the scheme for an unsteady problem and a domain discretized by overset grids with relative motion. Based on

these validations, the scheme is applied to a pitching-plunging NACA0005 airfoil at low Reynolds number, which is a simplified, two-dimensional representation of the flow around a flapping-wing-based micro air vehicle. The integrated forces are verified against previous computational results, and several improvements are observed in the resolution of the flowfield. The CRWENO5 scheme is then applied to two three-dimensional flow problems: the steady flow over the ONERA-M6 wing and the unsteady flow around the Harrington two-bladed rotor. Results are validated against experimental data, and the improvements in the resolution of the wake flowfield obtained with the CRWENO5 scheme are presented.

#### A. Steady Turbulent Flow over RAE2822 Airfoil

The CRWENO5 scheme is validated on a curvilinear mesh by solving the steady, transonic flow over the RAE2822 airfoil. The domain is discretized by a C-type,  $521 \times 401$  mesh with the outer boundary 50 chord lengths away. The wake contains 60 points in the wrap-around direction, and the grid spacing at the airfoil surface is  $4 \times 10^{-6}$  times the chord length. Freestream conditions are specified that correspond to “case 6” in the experimental database [49] for this airfoil. The chord-based Reynolds number is  $6.5 \times 10^6$ , the free-stream Mach number is 0.725, and the angle of attack is 2.92 deg. The angle of attack and freestream Mach number are corrected for wind-tunnel effects [50] to 2.51 deg and 0.731, respectively.

Characteristic boundary conditions are applied on outer boundaries, whereas no-slip conditions are enforced on the airfoil surface. Wake averaging is used in the wake-cut of the C-type mesh. Figure 1a shows the pressure contours and the velocity streamlines for the flowfield. The supersonic flow region on the upper surface and the shock that terminates it are clearly visible. Figure 1b shows the coefficient of pressure on the airfoil surface for the solution obtained by the CRWENO5 scheme. A good agreement is observed with the experimental data [49]. Figure 2 compares the velocity profiles at two locations: inside the boundary layer on the upper surface at  $x/c = 0.319$  and inside the wake at  $x/c = 1.025$ , and the numerical solution agrees well with the experimental data. Thus, the CRWENO5 scheme is validated for the steady flow over a domain discretized by a curvilinear grid. The density residual is shown in Fig. 3 for the CRWENO5 scheme as well as the WENO5 scheme. Although the solutions show good agreement with experimental data, both these schemes show residual drops of only one-and-a-half orders of magnitude. In this study, a componentwise reconstruction is used along with the nonlinear weights as formulated by Jiang and Shu [7]. The convergence of the WENO schemes for airfoil problems has been studied [51,52], and noncharacteristic-based formulations were observed to show poor convergence. A higher value of  $\epsilon = 10^{-2}$  in Eq. (16) has been proposed [51] that improves the convergence of the WENO scheme for this problem. However, this approach forces the nonlinear WENO scheme toward its underlying linear scheme, thus

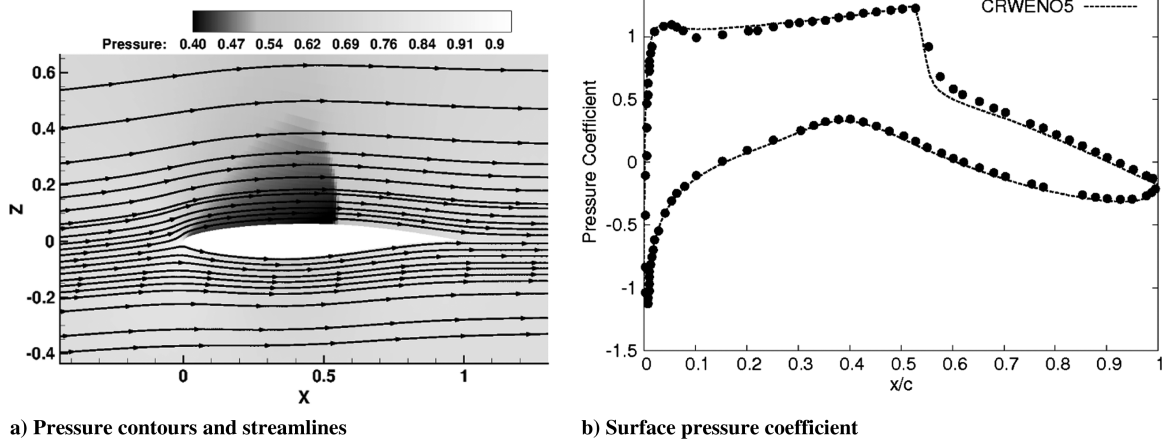


Fig. 1 Numerical solution to the transonic flow around the RAE2822 airfoil.

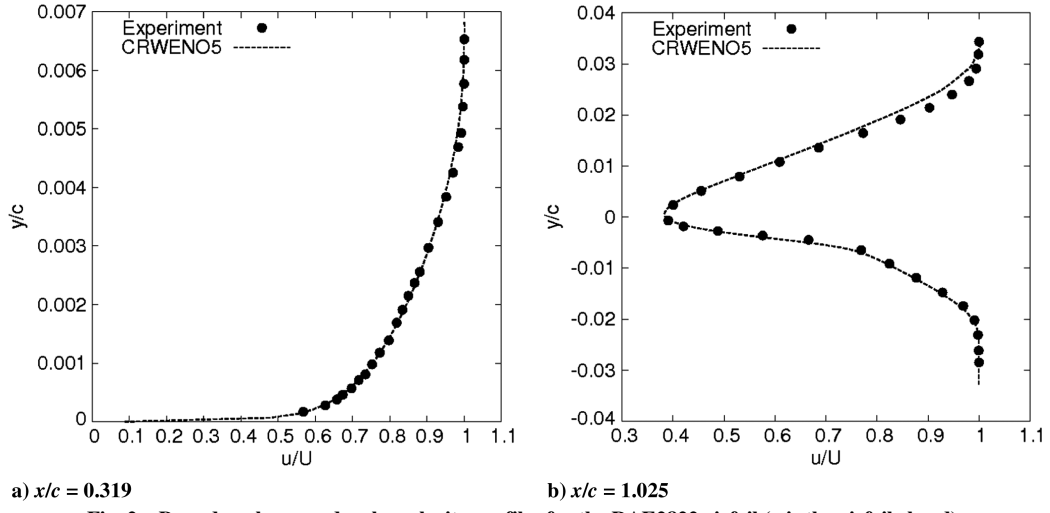
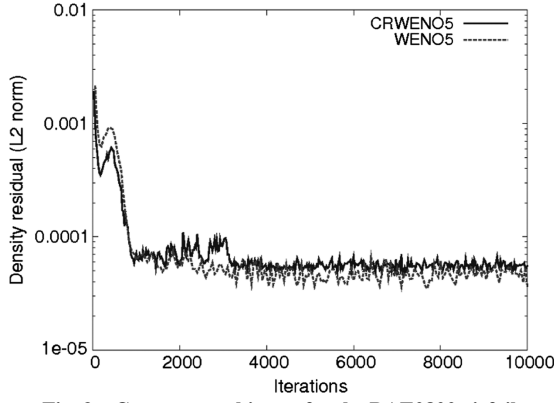
Fig. 2 Boundary-layer and wake-velocity profiles for the RAE2822 airfoil ( $c$  is the airfoil chord).

Fig. 3 Convergence history for the RAE2822 airfoil.

compromising its nonoscillatory nature. The value of  $\epsilon$  for which good convergence is achieved while retaining the nonoscillatory nature of the WENO scheme is problem-dependent. Thus, this approach is not considered in this study. Improvements to the convergence behavior for the CRWENO5 scheme is an area of active research.

#### B. Dynamic Stall of SC1095 Airfoil in Wind Tunnel

The CRWENO5 scheme is verified and validated for a domain discretized by overset grids with relative motion. The dynamic stall

of a pitching SC1095 airfoil in a wind tunnel is solved with the CRWENO5 as well as the noncompact MUSCL3 and WENO5 schemes. Figure 4a shows the domain discretized by the airfoil and wind-tunnel meshes, with the wind-tunnel height five times the airfoil chord length. A clustered Cartesian grid with  $151 \times 101$  points is used to discretize the wind tunnel, and a C-type,  $364 \times 138$  point grid is used around the airfoil, with the outer boundary approximately two chord lengths away. A wall spacing of  $5 \times 10^{-6}$  is used for the airfoil mesh, and no clustering is used for the wind-tunnel boundary layer. The region around the airfoil is blanked out for the wind-tunnel mesh, except near the outer boundaries of the airfoil mesh where it is coarser than the wind-tunnel mesh. The solution is exchanged through a bilinear interpolation in the overlap region.

The freestream Mach number of 0.302 and a chord-based Reynolds number of 3.92 million are specified. The airfoil pitches with a mean angle of attack of 9.78 deg, and the pitch amplitude is 9.9 deg at a reduced frequency of 0.099. The time step size for the simulations is taken at 0.01, which results in 10,500 iterations per cycle. Time-accurate solutions are obtained using dual-time stepping with 15 Newton subiterations. The simulation is run for four cycles, and solutions are compared for the last cycle. Figure 4b shows the lift as a function of the angle of attack over one complete cycle. The numerical solutions show a good agreement with experimental data. Figures 5a and 5b show the pressure contours around the airfoil at 18.83 deg angle of attack (upstroke) for solutions obtained with the CRWENO5 scheme and the WENO5 scheme, respectively. The vortices shed from the upper surface are transferred from the airfoil

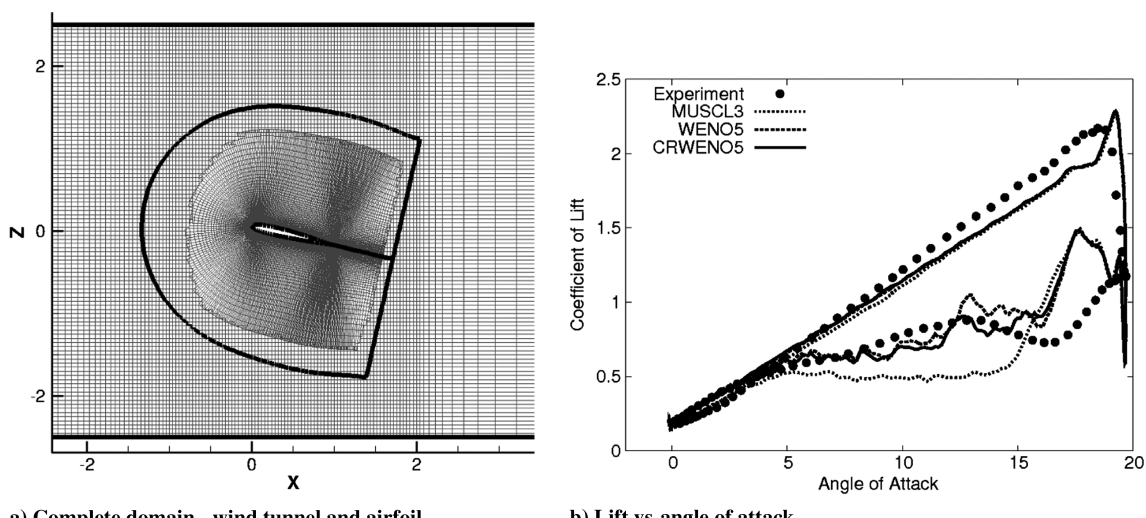
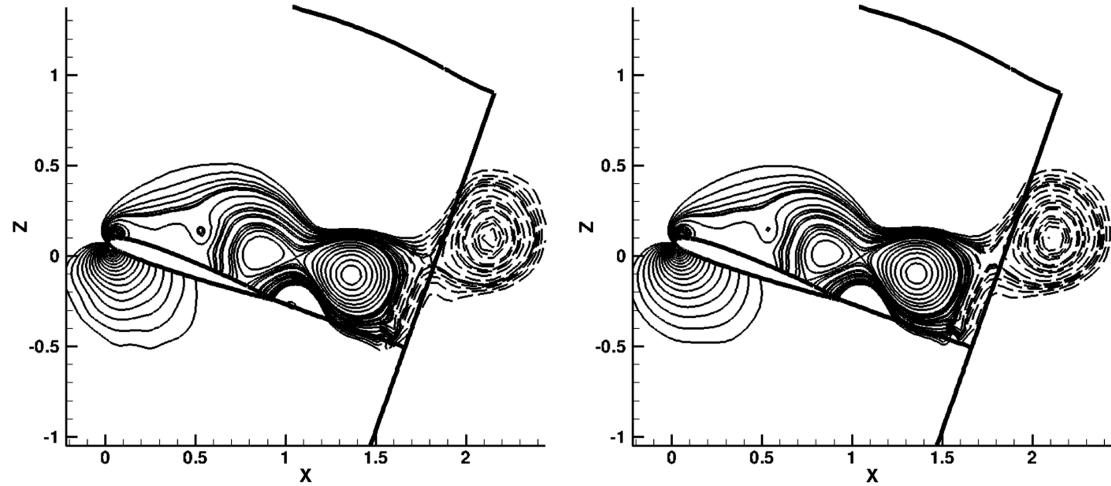


Fig. 4 Pitching SC1095 airfoil in a wind tunnel.



**Fig. 5** Comparison of pressure contours at 18.83 deg angle of attack for the overlap region: airfoil mesh (solid) and wind-tunnel mesh (dash).

mesh to the wind-tunnel mesh as they convect downstream, and the contours are continuous across the mesh boundaries. This verifies the performance of the CRWENO5 scheme for overset grids with blanked out regions and interpolation of flow data between the grids.

### C. Flow over Pitching–Plunging NACA0005 Airfoil

The flow around a pitching–plunging NACA0005 airfoil at a low Reynolds number is solved. It is a two-dimensional, simplified representation of the flow around a flapping-wing-based micro air vehicle and has been previously studied numerically using a second-order, incompressible RANS flow solver [53]. The airfoil motion generates a positive thrust (negative drag) and zero lift, averaged over one cycle. Lower-order algorithms are sufficient to accurately predict lift and thrust; this paper focuses on a well-resolved flowfield around the airfoil, including the formation and shedding of leading-edge vortical structures. In addition to the higher-order spatial schemes (CRWENO5 and WENO5), the one-equation Spalart–Allmaras turbulence model [32] is used with the delayed detached-eddy simulation modification in its two-dimensional form. It is expected that a higher-fidelity turbulence model with high-order accurate numerical scheme will improve the resolution of coherent vortical structures.

An O-type mesh with  $361 \times 361$  points is used to discretize the domain, with outer boundaries 45 chord lengths away. The free-stream, chord-based Reynolds number is 15,000, and the freestream Mach number is 0.1. The pitch amplitude is 40 deg with a zero mean angle of attack and a reduced frequency of 0.795. The plunging motion has an amplitude of 1.0 and the same reduced frequency but  $\pi/2$  behind in phase than the pitching motion. The airfoil pitches around the leading edge.

Time-accurate solutions are obtained using dual time stepping, with 15 Newton subiterations for each time step. A time step size of 0.008 is taken, resulting in 5000 iterations per cycle. The simulation is run for four cycles, and results are presented from the final cycle. Figure 6 shows the pressure distribution over one complete cycle for the solution obtained by the CRWENO5 scheme on the  $361 \times 361$  grid. As the airfoil plunges downward, leading-edge vortices are formed on the upper surface that grow in size and then detach from the surface. This results in a positive lift during the downstroke. Similarly, vortices form and shed from the lower surface during the upstroke, resulting in negative lift. This results in a zero average lift over the entire cycle. Both strokes result in negative drag, and the flapping motion causes the generation of positive thrust. The lift and drag variation over one cycle is shown in Fig. 7 for solutions obtained with the MUSCL3, WENO5, and CRWENO5 schemes as well as previous computational results [53]. The integrated forces agree well; however, some differences are observed with the previous results due to the differences in freestream conditions.

The numerical shadowgraph  $\nabla^2 \rho$  for the solutions during the upstroke ( $t/T = 0.75$ ) is shown in Fig. 8. The CRWENO5 schemes shows substantial improvements in the resolution of the wake and the leading-edge acoustic waves. Figure 9 shows the vorticity magnitude contours at  $t/T = 0.4$  for both the schemes, and the vortical structures shed from the upper surface are better resolved and preserved by the CRWENO5 scheme as they convect in the wake. Although the WENO5 and CRWENO5 schemes are both fifth-order accurate, the compact scheme is better able to resolve the unsteady flow features in the wake. Thus, to summarize, a lower-order scheme is sufficient to predict the integrated forces; however, a higher-order scheme is necessary to obtain a well-resolved flowfield around the airfoil. In this respect, the CRWENO5 scheme shows considerable improvements in the resolution of the solution, compared to the WENO5 scheme, with both being fifth-order accurate.

### D. Steady Flow over ONERA-M6 Wing

The CRWENO5 scheme is validated for a three-dimensional flow problem by solving the transonic flow around the ONERA-M6 wing. In addition, this problem is used to demonstrate and compare the ability of the scheme to preserve the tip vortices in the wake. Numerical solutions are usually obtained on a clustered mesh that stretch rapidly away from the body, and a high-order accurate numerical scheme is necessary to preserve the flow features as they convect in the wake. A single-block C-O mesh is used to discretize the domain, with 289 points in the wrap-around direction, 65 points in the normal direction, and 49 points in the spanwise direction. The wing has a unit semispan. Characteristic-based freestream boundary conditions are enforced at all far-field boundaries. No-slip wall boundary conditions are enforced on the wing surface. Symmetry is assumed on the plane corresponding to the wing root. The mean-aerodynamic-chord-based Reynolds number is 11.7 million, the angle of attack is 3.06 deg, and the freestream Mach number is 0.84.

The solution is marched in time until it reaches a steady state. It should be noted here that convergence issues, as described in Sec. IV.A, are observed for this problem too; however, acceptable solutions are obtained despite poor convergence. Figure 10 shows the pressure coefficient on the wing surface at various spanwise locations for the solution obtained by the CRWENO5 scheme and experimental data [54]. A good agreement is observed, thus validating the CRWENO5 scheme for a three-dimensional steady flow problem. The CRWENO5 scheme is compared to the WENO5 scheme with respect to their ability to accurately capture and preserve the tip vortex as it convects in the wake. Figure 11 shows the evolution of the tip vortex in the wake for the solutions obtained by the WENO5 and CRWENO5 schemes. The isosurface of the vorticity magnitude is shown in the figure. Near the wing, both the schemes are able to accurately capture the tip vortex and the solutions are similar.

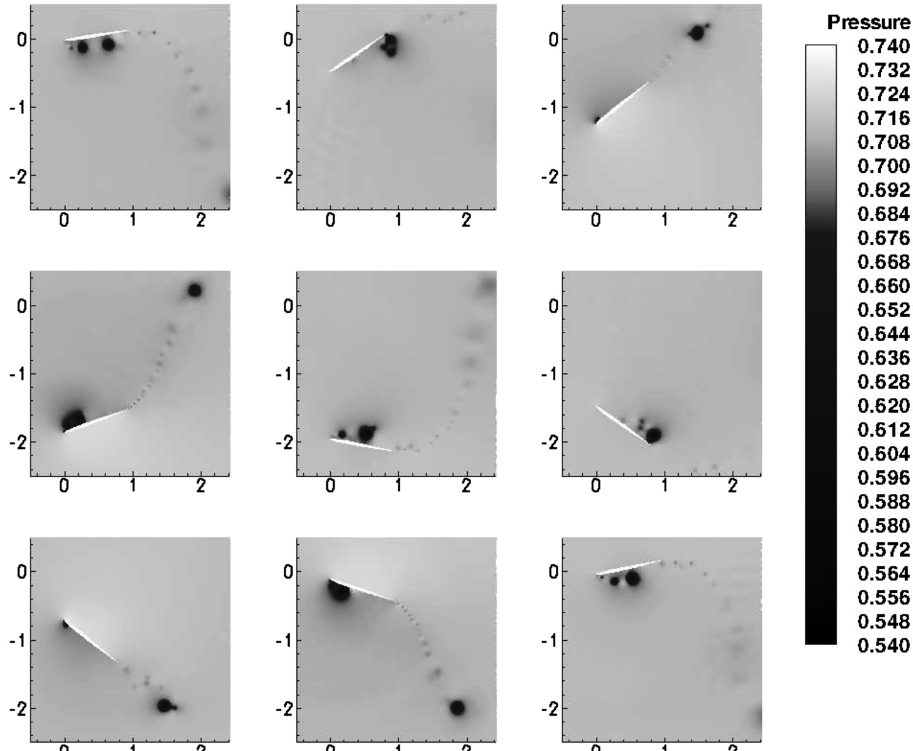


Fig. 6 Pressure distribution over one time period (ordering is from left to right and top to bottom).

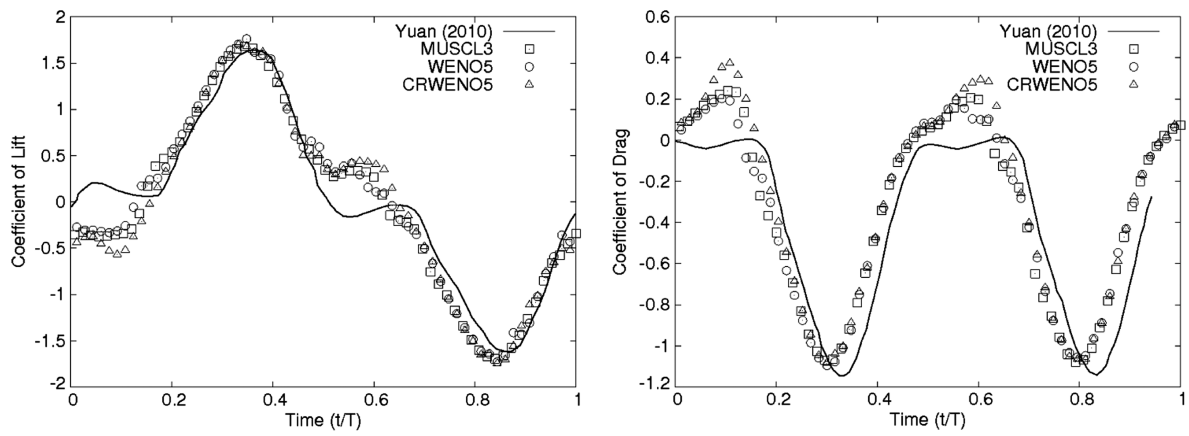


Fig. 7 Integrated forces over one time period.

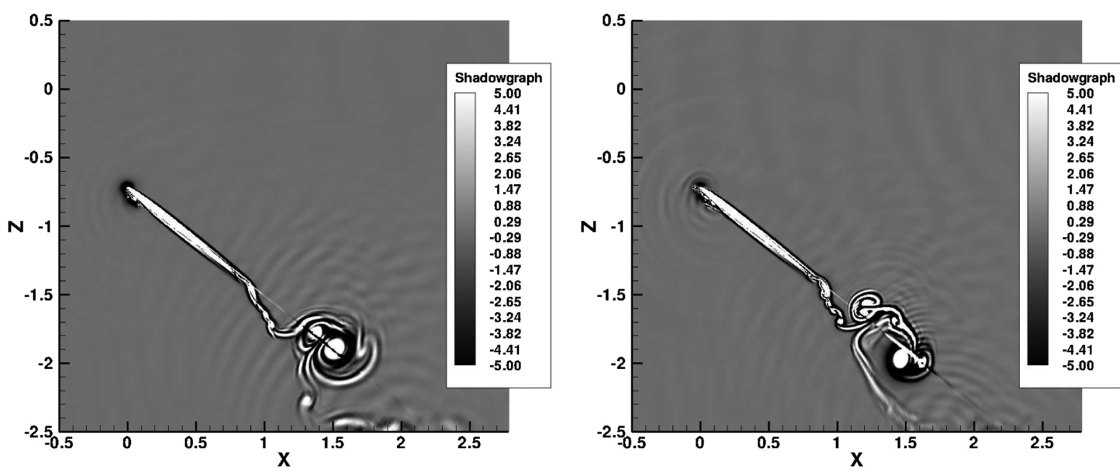


Fig. 8 Numerical shadowgraph for various schemes at  $t/T = 0.75$  (upstroke).

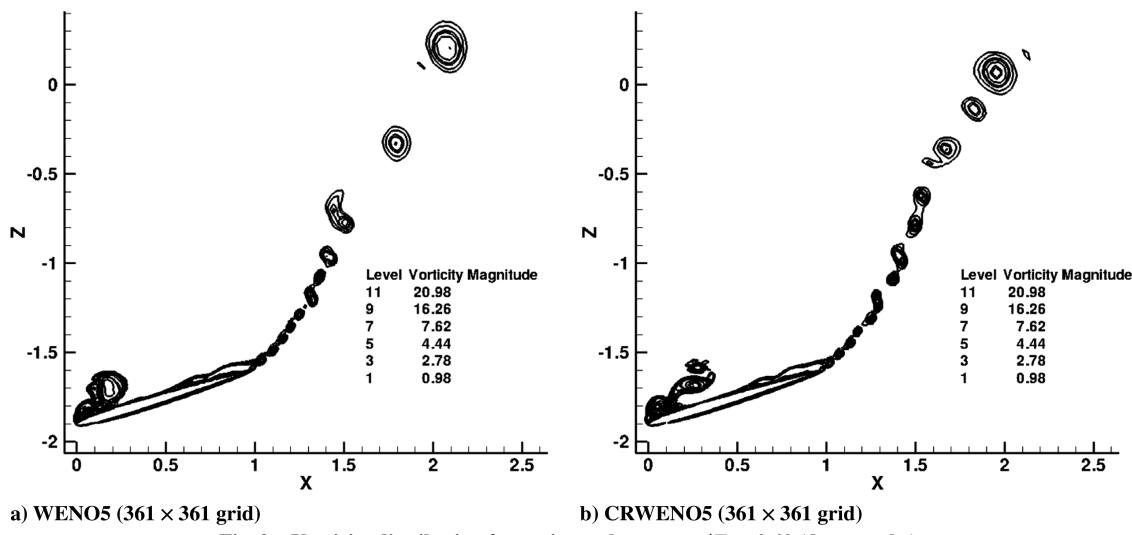
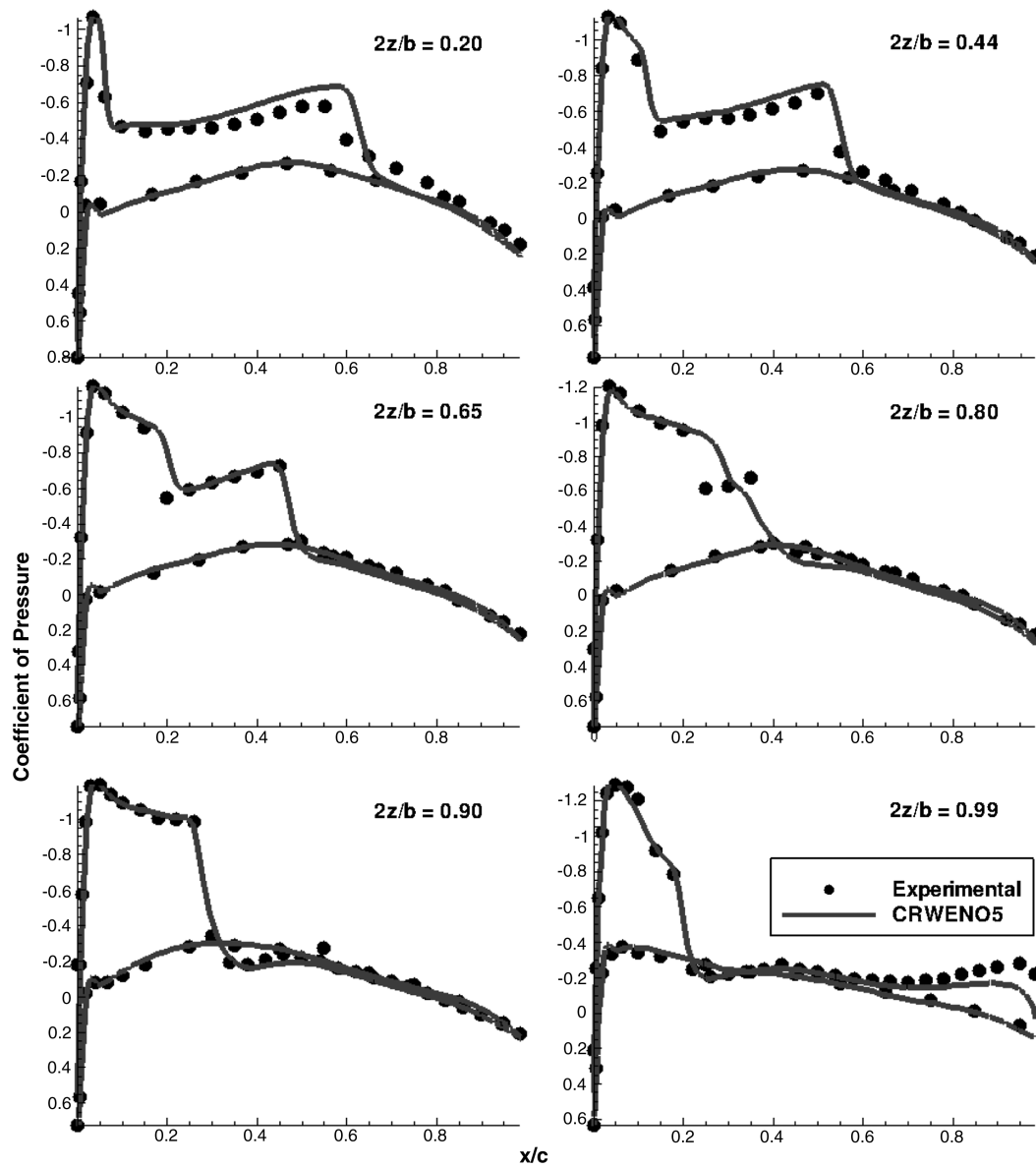
Fig. 9 Vorticity distribution for various schemes at  $t/T = 0.40$  (downstroke).

Fig. 10 Pressure coefficient on wing surface at various spanwise locations for the ONERA-M6 wing.

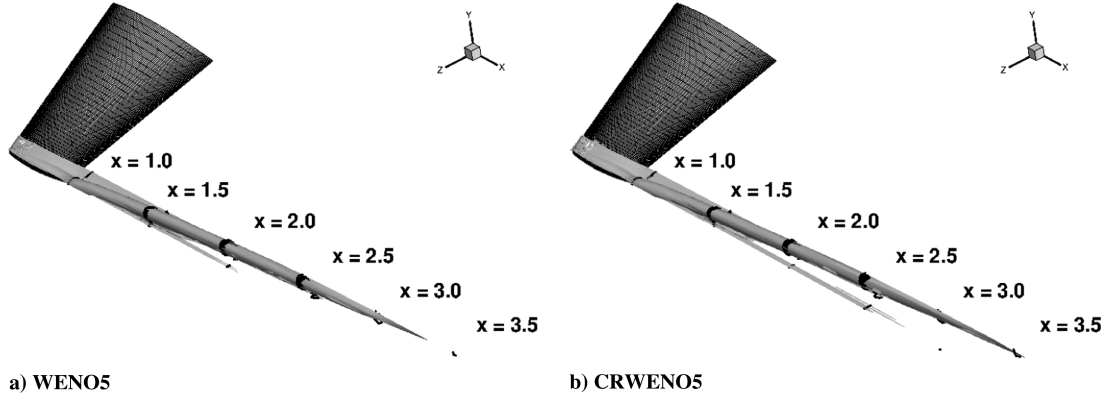
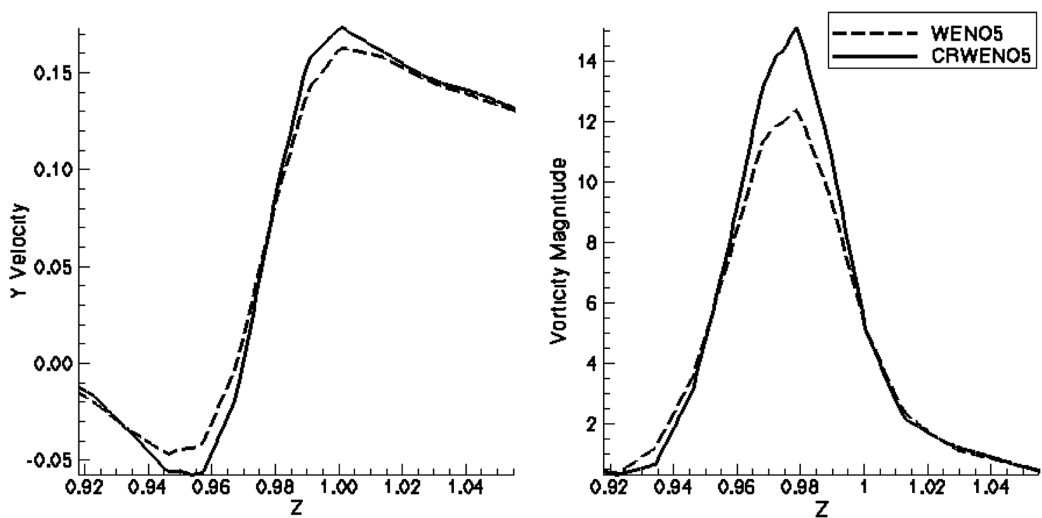


Fig. 11 Evolution of tip vortex in the wake for the ONERA-M6 wing.

Fig. 12 Comparison of swirl velocity and vorticity magnitude in the tip vortex at  $x = 1.5$ .

However, further downstream, the tip vortex is better preserved with the CRWENO5 scheme, as observed from the slices at  $x = 3.0$  and  $x = 3.5$ . Figure 12 compares the swirl velocity and vorticity magnitude through the tip vortex core at  $x = 1.5$ . The low dissipation of the CRWENO5 scheme yields a stronger vortex as it convects downstream in the wake.

#### E. Flow Around Harrington Rotor

The flow around the experimental Harrington two-bladed single rotor [55] is solved to validate the scheme for a three-dimensional unsteady flow on overset, moving grids. The flow around a rotor, and its wake, is dominated by the tip vortices shed from the blade.

A lower-order numerical scheme suffices to predict the integrated forces over the blades; however, a high-order accurate numerical scheme is required to resolve the wake and accurately capture the shed vortices as they convect away from the blades. It is demonstrated in this section that the CRWENO5 scheme results in substantial improvements in the resolution of wake flow features. The experimental setup referred to as “Rotor-2” [55] consists of a two-bladed rotor with an aspect ratio of 8.33 and is considered in this paper. The blade cross section is the symmetric NACA airfoil with a linearly varying thickness of 27.5% at the hub ( $0.2R$ ) to 15% at the tip ( $1.0R$ ), with  $R$  being the rotor radius. The tip Mach number and Reynolds number are 0.352 and  $3.5 \times 10^6$ , respectively. The collective pitch is

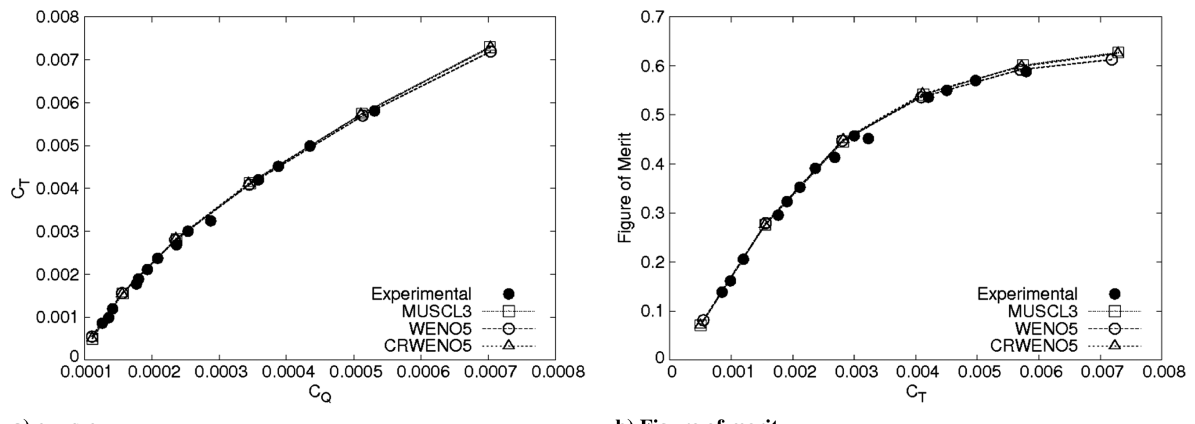
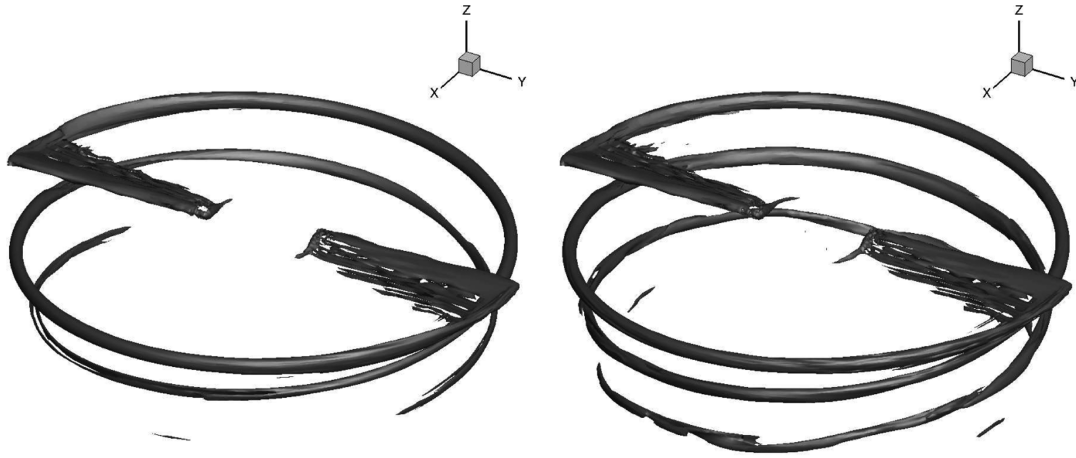


Fig. 13 Thrust and power coefficients, and the figure of merit, for the Harrington rotor.

varied from 2 to 12 deg to obtain the variation of thrust with power. The domain is discretized by a cylindrical background mesh with 127(radial)  $\times$  116(azimuthal)  $\times$  118(vertical) points, and a C-O-type blade mesh with 267.wrap-around  $\times$  78(span)  $\times$  56(normal) points. The background mesh is clustered near the blade mesh in the  $z$  direction and at the hub and tip regions in the radial direction. The

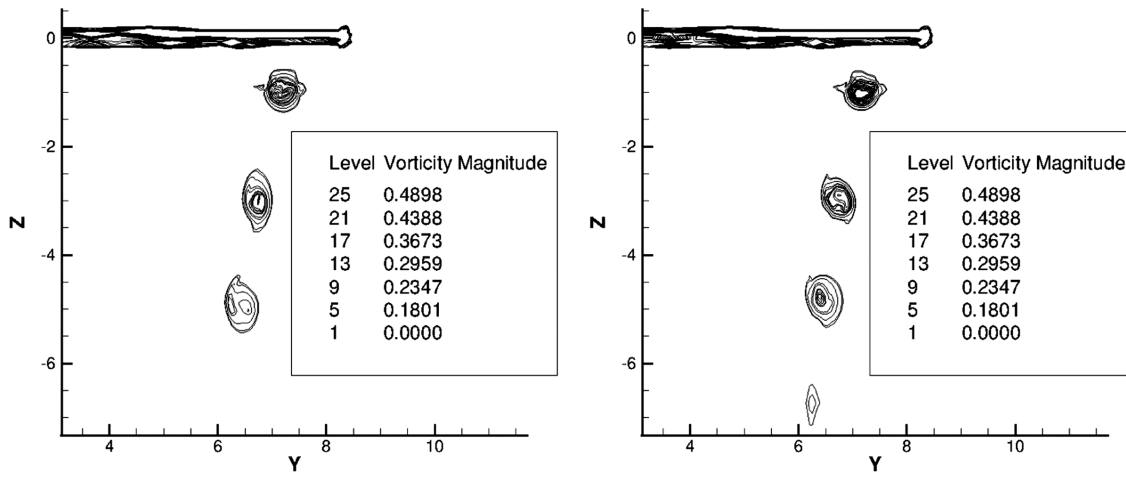
blade mesh is clustered at the hub and tip in the spanwise direction as well as the blade surface along the surface-normal direction. The solution is extrapolated with zero gradients at the center of the cylindrical mesh, while periodic boundary conditions are applied to the azimuthal boundaries. Characteristic-based freestream boundary conditions are applied at all other boundaries.



a) WENO5

b) CRWENO5

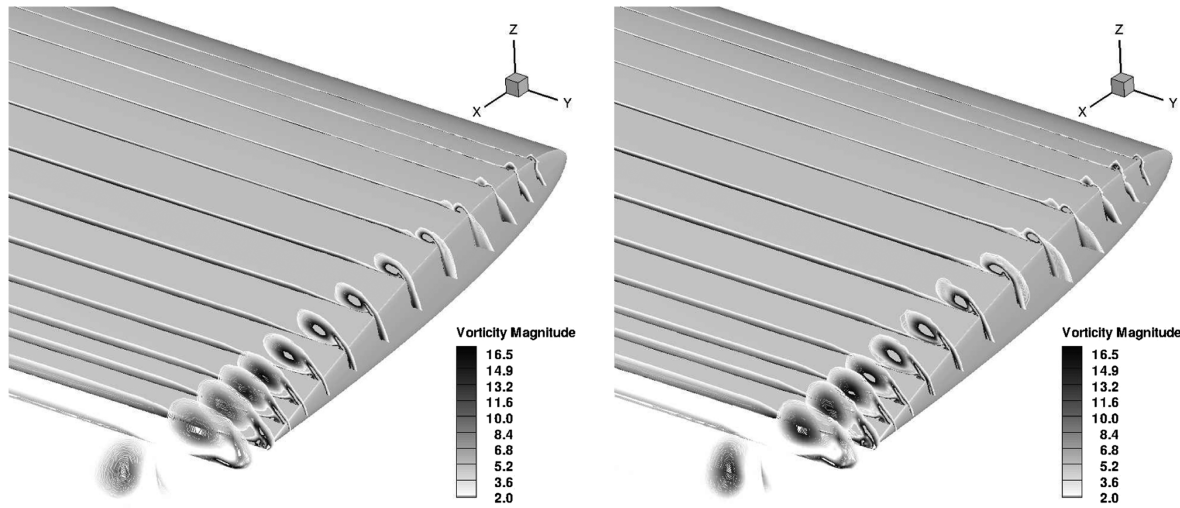
Fig. 14 Vorticity magnitude isosurfaces in the Harrington rotor wake flowfield.



a) WENO5

b) CRWENO5

Fig. 15 Vorticity magnitude contours on a cross-sectional slice at 0 deg azimuth.



a) WENO5

b) CRWENO5

Fig. 16 Comparison of the tip vortex for various numerical schemes.

Time-accurate solutions are obtained using dual time stepping with eight Newton subiterations. The simulations are carried out on eight processors using the message passing interface library (see Sec. III.E for a brief discussion on parallelization). Figure 13a shows the thrust coefficient as a function of the power coefficient for solutions obtained by the MUSCL3, WENO5, and CRWENO5 schemes, whereas Fig. 13b shows the figure of merit as a function of the thrust coefficient. The numerical solution agrees well with experimental data, thus validating the algorithm.

The ability of the CRWENO5 scheme to capture and preserve the helical tip vortex in the wake is compared to that of the WENO5 schemes. The lower dissipation and higher spectral resolution of the CRWENO5 scheme is expected to improve the resolution of the wake vortices in the wake. Figures 14 and 15 show isosurfaces of the vorticity magnitude in the wake and the vorticity magnitude contours on a cross-sectional slice at an azimuthal angle of 10 deg after 10 revolutions, respectively. In the figures showing the cross section of the wake, the first vortex below the blade has a wake age of  $\pi$  rad, the second vortex has a wake age of  $2\pi$  rad, and so forth. It is observed that the CRWENO5 scheme shows a substantial improvement in the preservation of the vortices as they convect through the domain. The shape and strength of the tip vortex is preserved until a wake age of  $3\pi$  in the solution obtained using the CRWENO5 scheme, whereas the vortex is significantly dissipated and distorted at this wake age for the solution obtained with the WENO5 scheme. Figure 16 shows the flow at the blade tip for the solutions obtained with the two schemes. The vorticity magnitude contours are shown at the various chordwise locations. The CRWENO5 scheme shows reduced dissipation and the formation of a stronger tip vortex. Thus, the CRWENO5 scheme improves the ability of the algorithm to accurately capture the tip vortices as they form and preserve their strength and structure as they convect in the wake.

## V. Conclusions

This paper describes the application of the compact-reconstruction WENO schemes to two- and three-dimensional, viscous flow problems on curvilinear and overset grids. Previous studies have demonstrated the advantages of the CRWENO scheme over the WENO scheme for benchmark inviscid flow problems on equispaced Cartesian grids. In this paper, the CRWENO scheme is integrated with a structured, finite-volume RANS solver and validated for two- and three-dimensional domains discretized by curvilinear grids. In addition, its performance is verified with noncompact schemes on overset grids with relative motion. Apart from validating and verifying the CRWENO scheme, flow problems are considered that are characterized by length scales ranging from airfoil chord length to core diameter of shed vortices. Lower-order numerical schemes (e.g., third-order MUSCL) are sufficient to predict the integrated forces; however, higher-order schemes (fifth-order WENO or CRWENO) are required to model relevant flow features in the solution. The ability of the CRWENO scheme to yield well-resolved solutions to such flows is demonstrated and compared with that of the WENO scheme. It is observed that the CRWENO scheme shows an improvement in capturing and preserving flow features such as shed vortices and boundary layers as well as resolving acoustic waves, compared to the WENO scheme of the same order of convergence. Thus, the CRWENO scheme is proposed as an efficient, high-resolution, non-oscillatory reconstruction scheme for subsonic and transonic aerodynamic flows, where a well-resolved solution to the flowfield is desired.

## Acknowledgments

This research was supported by the U.S. Army's Micro Autonomous Systems & Technology Collaborative Technology Alliance Center for Microsystem Mechanics with Chris Kroninger (Army Research Laboratory-Vehicle Technology Directorate) as Technical Monitor.

## References

- [1] Hirsch, C., *Numerical Computation of Internal and External Flows: The Fundamentals of Computational Fluid Dynamics*, Vols. 1–2, Elsevier Science, Burlington, MA, 2007, pp. 597–617.
- [2] Laney, C. B., *Computational Gasdynamics*, Cambridge Univ. Press, Cambridge, England, U.K., 1998, pp. 5–18.
- [3] Harten, A., "High Resolution Schemes for Hyperbolic Conservation Laws," *Journal of Computational Physics*, Vol. 49, No. 3, 1983, pp. 357–393.  
doi:10.1016/0021-9991(83)90136-5
- [4] Shu, C.-W., and Osher, S., "Efficient Implementation of Essentially Non-Oscillatory Shock-Capturing Schemes," *Journal of Computational Physics*, Vol. 77, No. 2, 1988, pp. 439–471.  
doi:10.1016/0021-9991(88)90177-5
- [5] Shu, C.-W., and Osher, S., "Efficient Implementation of Essentially Non-Oscillatory Shock-Capturing Schemes 2," *Journal of Computational Physics*, Vol. 83, No. 1, 1989, pp. 32–78.  
doi:10.1016/0021-9991(89)90222-2
- [6] Liu, X.-D., Osher, S., and Chan, T., "Weighted Essentially Non-Oscillatory Schemes," *Journal of Computational Physics*, Vol. 115, No. 1, 1994, pp. 200–212.  
doi:10.1006/jcph.1994.1187
- [7] Jiang, G.-S., and Shu, C.-W., "Efficient Implementation of Weighted ENO Schemes," *Journal of Computational Physics*, Vol. 126, No. 1, 1996, pp. 202–228.  
doi:10.1006/jcph.1996.0130
- [8] Balsara, D. S., and Shu, C.-W., "Monotonicity Preserving Weighted Essentially Non-Oscillatory Schemes with Increasingly High Order of Accuracy," *Journal of Computational Physics*, Vol. 160, No. 2, 2000, pp. 405–452.  
doi:10.1006/jcph.2000.6443
- [9] Henrick, A. K., Aslam, T. D., and Powers, J. M., "Mapped Weighted Essentially Non-Oscillatory Schemes: Achieving Optimal Order Near Critical Points," *Journal of Computational Physics*, Vol. 207, No. 2, 2005, pp. 542–567.  
doi:10.1016/j.jcp.2005.01.023
- [10] Borges, R., Carmona, M., Costa, B., and Don, W. S., "An Improved Weighted Essentially Non-Oscillatory Scheme for Hyperbolic Conservation Laws," *Journal of Computational Physics*, Vol. 227, No. 6, 2008, pp. 3191–3211.  
doi:10.1016/j.jcp.2007.11.038
- [11] Yamaeleev, N. K., and Carpenter, M. H., "A Systematic Methodology for Constructing High-Order Energy Stable WENO Schemes," *Journal of Computational Physics*, Vol. 228, No. 11, 2009, pp. 4248–4272.  
doi:10.1016/j.jcp.2009.03.002
- [12] Shu, C.-W., "High Order Weighted Essentially Nonoscillatory Schemes for Convection Dominated Problems," *SIAM Review*, Vol. 51, No. 1, 2009, pp. 82–126.  
doi:10.1137/070679065
- [13] Lele, S. K., "Compact Finite Difference Schemes with Spectral-Like Resolution," *Journal of Computational Physics*, Vol. 103, No. 1, 1992, pp. 16–42.  
doi:10.1016/0021-9991(92)90324-R
- [14] E, W., and Liu, J.-G., "Essentially Compact Schemes for Unsteady Viscous Incompressible Flows," *Journal of Computational Physics*, Vol. 126, No. 1, 1996, pp. 122–138.  
doi:10.1006/jcph.1996.0125
- [15] Wilson, R. V., Demuren, A. O., and Carpenter, M., "Higher-Order Compact Schemes for Numerical Simulation of Incompressible Flows," NASA CR-1998-206922, 1998.
- [16] Lerat, A., and Corre, C., "A Residual-Based Compact Scheme for the Compressible Navier-Stokes Equations," *Journal of Computational Physics*, Vol. 170, No. 2, 2001, pp. 642–675.  
doi:10.1006/jcph.2001.6755
- [17] Ekaterinaris, J. A., "Implicit, High-Resolution, Compact Schemes for Gas Dynamics and Aeroacoustics," *Journal of Computational Physics*, Vol. 156, No. 2, 1999, pp. 272–299.  
doi:10.1006/jcph.1999.6360
- [18] Cockburn, B., and Shu, C.-W., "Nonlinearly Stable Compact Schemes for Shock Calculations," *SIAM Journal on Numerical Analysis*, Vol. 31, No. 3, 1994, pp. 607–627.  
doi:10.1137/0731033
- [19] Yee, H. C., "Explicit and Implicit Multidimensional Compact High-Resolution Shock-Capturing Methods: Formulation," *Journal of Computational Physics*, Vol. 131, No. 1, 1997, pp. 216–232.  
doi:10.1006/jcph.1996.5608
- [20] Adams, N. A., and Shariff, K., "A High-Resolution Hybrid Compact-ENO Scheme for Shock-Turbulence Interaction Problems," *Journal of Computational Physics*, Vol. 127, No. 1, 1996, pp. 27–51.  
doi:10.1006/jcph.1996.0156
- [21] Pirozzoli, S., "Conservative Hybrid Compact-WENO Schemes for Shock-Turbulence Interaction," *Journal of Computational Physics*,

- Vol. 178, No. 1, 2002, pp. 81–117.  
doi:10.1006/jcph.2002.7021
- [22] Ren, Y.-X., Liu, M., and Zhang, H., “A Characteristic-Wise Hybrid Compact-WENO Scheme for Solving Hyperbolic Conservation Laws,” *Journal of Computational Physics*, Vol. 192, No. 2, 2003, pp. 365–386.  
doi:10.1016/j.jcp.2003.07.006
- [23] Shen, Y., and Zha, G., “Generalized Finite Compact Difference Scheme for Shock/Complex Flowfield Interaction,” *Journal of Computational Physics*, Vol. 230, No. 12, 2011, pp. 4419–4436.  
doi:10.1016/j.jcp.2011.01.039
- [24] Deng, X., and Zhang, H., “Developing High-Order Weighted Compact Nonlinear Schemes,” *Journal of Computational Physics*, Vol. 165, No. 1, 2000, pp. 22–44.  
doi:10.1006/jcph.2000.6594
- [25] Zhang, S., Jiang, S., and Shu, C.-W., “Development of Nonlinear Weighted Compact Schemes with Increasingly Higher Order Accuracy,” *Journal of Computational Physics*, Vol. 227, No. 15, 2008, pp. 7294–7321.  
doi:10.1016/j.jcp.2008.04.012
- [26] Wang, Z., and Huang, G. P., “An Essentially Nonoscillatory High-Order Padé-Type (ENO-Padé) Scheme,” *Journal of Computational Physics*, Vol. 177, No. 1, 2002, pp. 37–58.  
doi:10.1006/jcph.2002.6998
- [27] Jiang, L., Shan, H., and Liu, C., “Weighted Compact Scheme for Shock Capturing,” *International Journal of Computational Fluid Dynamics*, Vol. 15, No. 2, 2001, pp. 147–155.  
doi:10.1080/10618560108970024
- [28] Liu, C., Jiang, L., Visbal, M., and Xie, P., “Smart Weighted Compact Scheme for Shock Tube and Shock-Entropy Interaction” *36th AIAA Fluid Dynamics Conference and Exhibit*, AIAA Paper 2006-3708, June 2006,  
doi:10.2514/6.2006-3708
- [29] Xie, P., and Liu, C., “Weighted Compact and Non-Compact Scheme for Shock Tube and Shock Entropy Interaction,” *45th AIAA Aerospace Sciences Meeting and Exhibit*, AIAA Paper 2007-0509, Jan. 2007,  
doi:10.2514/6.2007-509
- [30] Ghosh, D., and Baeder, J. D., “Compact Reconstruction Schemes with Weighted ENO Limiting for Hyperbolic Conservation Laws,” *SIAM Journal on Scientific Computing*, Vol. 34, No. 3, 2012, pp. 1678–1706.  
doi:10.1137/110857659
- [31] Ghosh, D., and Baeder, J. D., “Weighted Non-Linear Compact Schemes for the Direct Numerical Simulation of Compressible, Turbulent Flows,” *Journal of Scientific Computing* (in press).  
doi:10.1007/s10915-014-9818-0
- [32] Spalart, P., and Allmaras, S., “A One-Equation Turbulence Model for Aerodynamic Flows,” *30th Aerospace Sciences Meeting and Exhibit*, AIAA Paper 1992-0439, Jan. 1992.  
doi:10.2514/6.1992-439
- [33] Dacles-Mariani, J., Zilliac, G. G., Chow, J. S., and Bradshaw, P., “Numerical/Experimental Study of a Wingtip Vortex in the Near Field,” *AIAA Journal*, Vol. 33, No. 9, 1995, pp. 1561–1568.  
doi:10.2514/3.12826
- [34] LeVeque, R. J., “Finite Volume Methods for Hyperbolic Problems,” *Cambridge Texts in Applied Mathematics*, Cambridge Univ. Press, Cambridge, England, U.K., 2002, pp. 64–84.
- [35] Warming, R. F., and Beam, R. M., “On the Construction and Application of Implicit Factored Schemes for Conservation Laws,” *SIAM-AMS Proceedings*, Vol. 11, 1978, pp. 85–129.
- [36] Pulliam, T. H., and Chaussee, D. S., “A Diagonal Form of an Implicit Approximate-Factorization Algorithm,” *Journal of Computational Physics*, Vol. 39, No. 2, 1981, pp. 347–363.  
doi:10.1016/0021-9991(81)90156-X
- [37] Jameson, A., and Yoon, S., “Lower-Upper Implicit Schemes with Multiple Grids for the Euler Equations,” *AIAA Journal*, Vol. 25, No. 7, 1987, pp. 929–935.  
doi:10.2514/3.9724
- [38] Yoon, S., and Jameson, A., “Lower-Upper Symmetric-Gauss-Seidel Method for the Euler and Navier-Stokes Equations,” *AIAA Journal*, Vol. 26, No. 9, 1988, pp. 1025–1026.  
doi:10.2514/3.10007
- [39] Pulliam, T., “Time Accuracy and the Use of Implicit Methods,” *11th Computational Fluid Dynamics Conference*, AIAA Paper 1993-3360, 1993.
- [40] Roe, P. L., “Approximate Riemann Solvers, Parameter Vectors, and Difference Schemes,” *Journal of Computational Physics*, Vol. 43, No. 2, 1981, pp. 357–372.  
doi:10.1016/0021-9991(81)90128-5
- [41] Rothe, A., “Eigenvalues and Eigenvectors of the Euler Equations in General Geometries,” *15th AIAA Computational Fluid Dynamics Conference*, AIAA Paper 2001-2609, June 2001,  
doi:10.2514/6.2001-2609
- [42] van Leer, B., “Towards the Ultimate Conservative Difference Scheme. 2: Monotonicity and Conservation Combined in a Second-Order Scheme,” *Journal of Computational Physics*, Vol. 14, No. 4, 1974, pp. 361–370.  
doi:10.1016/0021-9991(74)90019-9
- [43] Koren, B., *A Robust Upwind Discretization Method for Advection, Diffusion and Source Terms*, Centrum voor Wiskunde en Informatica, Amsterdam, 1993.
- [44] Ghosh, D., “Compact-Reconstruction Weighted Essentially Non-Oscillatory Schemes for Hyperbolic Conservation Laws,” Ph.D. Thesis, Univ. of Maryland, College Park, MD, 2013.
- [45] Lee, Y., and Baeder, J. D., “Implicit Hole Cutting—A New Approach to Overset Grid Connectivity,” *16th AIAA Computational Fluid Dynamics Conference*, AIAA Paper 2003-4128, June 2003,  
doi:10.2514/6.2003-4128
- [46] Sherer, S. E., and Scott, J. N., “High-Order Compact Finite-Difference Methods on General Overset Grids,” *Journal of Computational Physics*, Vol. 210, No. 2, 2005, pp. 459–496.  
doi:10.1016/j.jcp.2005.04.017
- [47] Chao, J., Haselbacher, A., and Balachandar, S., “A Massively Parallel Multi-Block Hybrid Compact-WENO Scheme for Compressible Flows,” *Journal of Computational Physics*, Vol. 228, No. 19, 2009, pp. 7473–7491.  
doi:10.1016/j.jcp.2009.07.005
- [48] Ghosh, D., Constantinescu, E., and Brown, J., “Scalable Non-Linear Compact Schemes,” Argonne National Lab. TR ANL/MCS-TM-340, Lemont, IL, 2014.
- [49] Cook, P. H., Firmin, M. C. P., and McDonald, M. A., *Aerofoil RAE 2822: Pressure Distributions, and Boundary Layer and Wake Measurements*, RAE, 1977, p. 113.
- [50] Tatsumi, S., Martinelli, L., and Jameson, A., “A New High Resolution Scheme for Compressible Viscous Flows with Shocks,” *33rd Aerospace Sciences Meeting and Exhibit*, AIAA Paper 1995-0466, Jan. 1995.
- [51] Shen, Y., Zha, G., and Wang, B., “Improvement of Stability and Accuracy for Weighted Essentially Nonoscillatory Scheme,” *AIAA Journal*, Vol. 47, No. 2, 2009, pp. 331–344.  
doi:10.2514/1.37697
- [52] Su, X., Sasaki, D., and Nakahashi, K., “Efficient Implementation of WENO Scheme on Structured Meshes,” *Proceedings of the 25th Computational Fluid Dynamics Symposium*, Japan Society of Fluid Mechanics, Osaka, 2011, available online at [http://www2.nagare.or.jp/cfd/cfd25/webproc\\_paper/C01-3.pdf](http://www2.nagare.or.jp/cfd/cfd25/webproc_paper/C01-3.pdf).
- [53] Yuan, W., Lee, R., Hoogkamp, E., and Khalid, M., “Numerical and Experimental Simulations of Flapping Wings,” *International Journal of Micro Air Vehicles*, Vol. 2, No. 3, 2010, pp. 181–208.  
doi:10.1260/1756-8293.2.3.181
- [54] Schmitt, V., and Charpin, F., “Pressure Distributions on the ONERA-M6-Wing at Transonic Mach Numbers,” Office National d’Etudes et Recherches Aerospatiales TR-92320, Chatillon, France, 1979.
- [55] Harrington, R., *Full-Scale-Tunnel Investigation of the Static-Thrust Performance of a Coaxial Helicopter Rotor*, NACA TN-2234, 1951.

G. Blaisdell  
Associate Editor